Mon. Not. R. Astron. Soc. **000**, 000–000 (0000) Printed 11 March 2010 (MN LATEX style file v2.2)

Spatial structure of X-ray filaments in SN 1006

G. Morlino[1,2,3⋆], E. Amato[1,3] †, P. Blasi[1,3]‡, and D. Caprioli[1,2,3]§,
[1] *INAF/Osservatorio Astrofisico di Arcetri, Firenze, Italy*
[2] *Physics Department, North Carolina State University, Box 8202, Raleigh, NC 27695*
[3] *Kavli Institute for Theoretical Physics, Kohn Hall Santa Barbara, CA 93106-0001, USA*

Accepted 2010 March 10. Received 2010 March 10; in original form 2009 December 15

ABSTRACT
The theory of Non-Linear Diffusive Shock Acceleration (NLDSA) predicts the formation of a precursor upstream of the shock, where accelerated particles diffuse and induce magnetic field amplification through streaming instability. The non detection of this precursor in X-rays in *Chandra* observations of the north-eastern region of SN 1006 (G329.6+14.6) led to impose an upper limit to the X-ray emission generated by accelerated electrons diffusing in this precursor, at an emissivity level of < 1.5 per cent of the emission from the downstream region (Long et al. 2003). This has been used as an argument against Fermi acceleration at this shock. Here we calculate the spectrum and spatial distribution of accelerated particles in SN 1006 and show that *Chandra* results (including more recent data) are in perfect agreement with the predictions of NLDSA suggesting efficient particle acceleration and magnetic field amplification upstream of the shock by a factor ~ 10.

Key words: X-ray – supernova remnant – particle acceleration – shock waves – magnetic field amplification

1 INTRODUCTION

The blast waves produced by supernova remnants (SNRs) expanding in the interstellar medium (ISM) are thought to be the sites where the bulk of Galactic cosmic rays (CR) are accelerated. The simplest conversion mechanism of kinetic energy of the expanding plasma into accelerated particles is Diffusive Shock Acceleration (DSA). Narrow rims of non-thermal X-ray emission, associated with the outer shocks of several young SNRs (see e.g. Parizot et al. 2006, and references therein), are commonly interpreted as due to synchrotron emission radiated by $\sim$ TeV electrons (for the case of SN 1006 see Bamba et al. 2003). These X-ray filaments might also represent an indirect evidence of efficient acceleration of ions at the same shocks, since their thickness is most easily explained in terms of severe synchrotron losses of electrons in intense magnetic fields (in the range 100-500 μG, Ballet 2006), to be compared with the ISM magnetic field, $\sim 3\mu$G. In order to account for this difference, it has been proposed that magnetic fields are amplified in the shock region by the streaming of cosmic ray ions. This gives rise to an interesting scenario in which magnetic fields are generated by cosmic rays while in turn making CR acceleration more efficient in a complex chain of non linear effects. If indeed the magnetic field amplification (MFA) is due to CR streaming, this may happen either via resonant (Skilling 1975) or non-resonant instabilities (Bell 2004), though many variations on the theme are possible. The peculiarity of CR induced MFA is that it occurs upstream of the shock thereby reducing the acceleration time. On the other hand MFA could also be generated downstream by fluid instabilities (e.g. Giacalone & Jokipii 2007) induced by the shock corrugation while propagating in a inhomogeneous medium. Finally the narrow filaments might be due to damping of the magnetic field (Pohl et al. 2003) rather than to severe synchrotron losses, although correspondingly thin filaments in the radio emission do not seem to be observed (Rothenflug et al. 2004). The only way to discriminate among these different scenarios is through extensive comparison between theory and data.

The spatial profile of the X-ray brightness around the shock provides invaluable information on the acceleration mechanism and the magnetic field generation. Based on the non detection of X-rays with *Chandra* from the upstream region of the north-eastern limb of SN 1006, Long et al. (2003) concluded that any X-ray halo upstream must be at least a factor ~ 70 fainter than the peak brightness of the shell. Based on this finding, these authors suggested that Fermi acceleration is not the acceleration mechanism at work or that the jump in magnetic field at the shock is $\gg 4$. They

⋆ E-mail: morlino@arcetri.astro.it
† E-mail: amato@arcetri.astro.it
‡ E-mail: blasi@arcetri.astro.it; blasi@fnal.gov
§ E-mail: caprioli@arcetri.astro.it

also question the possibility that observations may be explained by the non linear theory of DSA.

In this Letter we apply the theory of NLDSA to show that its predictions provide an excellent description of *Chandra* observations, which in turn may be used to constrain the acceleration efficiency in SN 1006. A previous attempt at using the same technique was made in (Berezhko et al. 2003), where a different filament was studied and some aspects of the theory were treated in a more simplified way (for instance self-consistent, space dependent MFA in the precursor was not accounted for).

2 NLDSA MODEL FOR SN 1006

In NLDSA theory, the overall shock structure and the outcome of the particle acceleration process are inextricably linked. When acceleration is efficient, the pressure of accelerated particles affects the shock dynamics, leading to the formation of a precursor, namely a region where the fluid velocity progressively decreases while approaching the shock from far upstream. This causes the total compression factor between upstream infinity and downstream to exceed 4. At the same time the streaming of accelerated particles is responsible for instabilities that lead to MFA. In turn, the fluid profile in the precursor and the amplified, turbulent magnetic field, with the scattering it provides (and possibly the induced energy losses), determine the efficiency of particle acceleration and the resulting spectrum, including its high energy cutoff.

Here the shock structure and the accelerated particle spectrum are computed as in Morlino et al. (2009): the basic structure of the calculation is that proposed by Amato & Blasi (2005, 2006), but the conservation equations are modified so as to also take into account the dynamical reaction of the self-generated magnetic field (Caprioli et al. 2009). The compressibility of the overall fluid is deeply affected by the magnetic contribution as soon as the magnetic field pressure becomes comparable to the thermal pressure upstream. The net result is that the total compression ratio between downstream and upstream infinity, $R_{tot} = u_0/u_2$, decreases with respect to the case in which this dynamical backreaction is neglected, thereby leading to a smoother precursor and accelerated particle spectra that are less concave and closer to power-laws.

The normalization of the proton spectrum is an output of our non linear calculation, once a recipe for injection in the acceleration process is established. Here we follow Blasi, Gabici & Vannoni (2005), and assume that the fraction of injected particles, $\eta_{\rm inj}$, is

$$\eta_{\rm inj} = 4/\left(3\sqrt{\pi}\right)(R_{\rm sub}-1)\,\xi^3\,e^{-\xi^2}\,. \quad (1)$$

where $R_{sub} = u_1/u_2$ is the compression ratio at the subshock and $\xi \sim 2-4$ is the ratio between the injection momentum and the momentum of thermal particles downstream, $p_{\rm th,2}$. While ξ parametrizes the poorly known microphysics of the injection process, $p_{\rm th,2}$ is an output of the calculation: as a result, the injection efficiency is affected by the dynamical reaction of both particles and fields.

Energy losses are not important for accelerated protons, so that their maximum energy is obtained by equating the acceleration time and the age of the remnant, $t_{acc}(p_{p,\rm max}) = t_{\rm SNR}$ (Blasi et al. 2007). For electrons the maximum energy is reached when the acceleration time equals the minimum between the age of the remnant and the loss time scale, τ_l, weighed by the residence times, t_r, upstream and downstream of the shock (subscripts 1 and 2 respectively), over one cycle:

$$t_{acc}(p) = [t_{r,1}(p)+t_{r,2}(p)]\left[\frac{t_{r,1}(p)}{\tau_{l,1}(B_1,p)}+\frac{t_{r,2}(p)}{\tau_{l,2}(B_2,p)}\right]^{-1}\,. (2)$$

Once $t_{r,1}$ and $t_{r,2}$ are written explicitly in the context of NLDSA (from Eqs. (25) and (26) of Blasi et al. 2007), Eq. (2) must be solved numerically for $p_{e,\rm max}$. The following approximate analytical solution can be found when only synchrotron losses are relevant (Morlino et al. 2009, Eq. (4)):

$$p_{e,\rm max} = 137\,H(p_{e,\rm max})\left(\frac{B_1}{\mu\rm G}\right)^{-\frac{1}{2}}\left(\frac{u_0}{3000\,\rm km/s}\right)\frac{\rm TeV}{\rm c}\,. \quad (3)$$

Here $H(p)$ is a function of the shock modification taking into account the mean plasma speed, $u_p = u_0 U_p(p)$, that a particle with momentum p experiences in the precursor (see Eq. (8) of Amato & Blasi (2005) and Eq. (4) of Morlino et al. (2009)). Here $H(p)$ is normalized in such a way that $H(p) = 1$ in the test-particle limit.

The electron spectrum at the shock, $f_{e,0}(p)$, follows the proton spectrum for $p \ll p_{e,\rm max}$, provided the diffusion coefficient is the same for both species. The normalization of the electron spectrum relative to the proton spectrum, K_{ep}, is instead unconstrained from the dynamics, since electrons have no dynamical role, and can only be derived from observations.

The electron spectrum at energies around and above $p_{e,\rm max}$, namely the shape of the cutoff, has never been computed in the context of NLDSA. Since the spectra we find for electrons at $p < p_{e,\rm max}$ are not far from being power laws with slope ~ 4, we adopt the modification factor calculated by Zirakashvili & Aharonian (2007) for strong shocks in the test particle regime. The resulting electron spectrum at the shock, in the loss dominated case, is:

$$f_{e,0}(p) = K_{ep}\,f_{p,0}(p)\left[1+0.523\,(p/p_{e,\rm max})^{\frac{9}{4}}\right]^2 e^{-p^2/p^2_{e,\rm max}}\,. (4)$$

An important point to notice in Eq. (4) is that the cutoff is super-exponential, which reflects in the shape of the synchrotron spectrum, making it different from what is assumed in most of the previous work on the subject. On the other hand, if the maximum momentum is determined by the age of the remnant, then the cutoff shape is a simple exponential.

While a few different mechanisms have been proposed for MFA at SNR shocks, here we focus on the waves that are resonantly excited (Skilling 1975) upstream by the streaming of cosmic rays accelerated at the shock. While streaming cosmic rays can excite very effectively also non-resonant modes (Bell 2004), these are likely dominant only at early times, while after the beginning of the Sedov phase MFA is mostly due to resonant waves (Amato & Blasi 2009). Moreover the role of these non resonant modes for scattering the particles is yet to be clarified.

When the predictions of linear theory are extrapolated to the non-linear regime of MFA (which one is forced to do for lack of a better treatment), the resulting field strengths

are in agreement with the values inferred by identifying the thickness of the X-ray filaments with the synchrotron loss length of the highest energy electrons. The strength of the magnetic field at the position x upstream, $\delta B(x)$, in the absence of damping, can be estimated from the saturation condition. For modified shocks this reads (Caprioli et al. 2009, Eq. (43)):

$$\frac{\delta B(x)^2}{8\pi\rho_0 u_0^2} = U(x)^{-3/2}\left[\frac{1-U(x)^2}{4\,M_{A,0}}\right], \quad (5)$$

where the *lhs* is the turbulent magnetic pressure normalized to the incoming momentum flux at upstream infinity, $U(x) = u(x)/u_0$ is the normalized velocity profile in the precursor, and $M_{A,0} = u_0/v_A$ with v_A the Alfvén velocity at upstream infinity, where only the background magnetic field, B_0, assumed parallel to the shock normal, enters. Eq. (5) correctly describes the effect of compression in the shock precursor through the term $U(x)^{-3/2}$.

The magnetic field downstream of the subshock is further enhanced by compression, so that $B_2 = R_B\,B_1$, where B_1 is the magnetic field immediately upstream of the subshock and, for Alfvèn waves (turbulence perpendicular to the shock normal), $R_B = R_{sub}$. We neglect any kind of magnetic damping both in the upstream and in the downstream region.

3 THE SIZE OF THE X-RAY FILAMENTS

SN 1006 is one of the best suited remnants for the study of the spatial profile of X-ray emission since its non-thermal rims, with a typical thickness of 30"-40", are well resolved by *Chandra*, whose angular resolution is $\Delta\phi \sim 1''$. The spatial resolution corresponding to this value of $\Delta\phi$, $\Delta x = 3\times10^{16}\,(d/2\,\mathrm{kpc})\,(\Delta\phi/\mathrm{arcsec})\,\mathrm{cm}$ on a source at a distance d, has to be compared with the extension of the region in the upstream (downstream) fluid where electrons radiate at the observed frequency ν_0, i.e. $\Delta R_{1(2)}(\nu_0)$. Before illustrating the results of the detailed calculation, we provide some simple but useful approximate relations.

In the upstream region electrons diffuse up to a distance $L_{\rm diff} = D(p)/u_p(p)$ from the shock, where D is the diffusion coefficient and u_p is the effective fluid velocity experienced by particles with momentum p. The spatial distribution of electrons, $f_1(p)$, is roughly constant up to the diffusion length $L_{\rm diff}$, and is then cut off (Blasi 2009). Assuming Bohm diffusion, $D_B = pc^2/(3eB)$, we find:

$$\Delta R_1(\nu) \simeq L_{\rm diff}(h\nu) = \frac{D_B(p)}{u_p(p)} = \frac{pc^2}{3eB_1 u_p(p)} = 9\times10^{17}\left(\frac{h\nu}{1\,\mathrm{keV}}\right)^{\frac{1}{2}}\left(\frac{B_1}{10\,\mu\mathrm{G}}\right)^{-\frac{3}{2}}\left(\frac{u_0\,U_p(p)}{3000\,\mathrm{km/s}}\right)^{-1}\mathrm{cm}, \quad (6)$$

where we used the fact that synchrotron emission of electrons with energy E in a μG field peaks at energy $h\nu = 1.5\times10^{-2}B_{\mu\mathrm{G}}\,{E_{\mathrm{TeV}}}^2\mathrm{eV}$. Since $L_{\rm diff}$ strongly depends on the magnetic field strength, the possibility of resolving the upstream X-ray halo depends on the level of upstream MFA.

In the upstream region, electrons with $E = E_{\rm max}$ radiate at a typical frequency

$$h\nu_1 = 0.28\,H(p_{e,\rm max})(u_0/3000\mathrm{km\ s^{-1}})^2\ \mathrm{keV}, \quad (7)$$

where we used the expression in Eq. (3) for $E_{\rm max}$. Clearly Eq. (6) holds only for $E < E_{max}$, since at higher energies the diffusion region upstream becomes regulated by synchrotron losses:

$$\Delta R_1(\nu > \nu_1) \simeq L_{\rm diff}(h\nu_1)\ . \quad (8)$$

The size of the radiating region downstream is determined by the competition between advection and diffusion of the electrons during their life-time, namely $L^{\rm loss}_{\rm adv} = u_2\,\tau_l(p) \propto p^{-1}$ and $L^{\rm loss}_{\rm diff} = \sqrt{D(p)\,\tau_l(p)}$ (the latter is independent of energy for Bohm diffusion). These two length-scales are equal for particle momenta corresponding to photon energy:

$$h\nu_2 = 1.00\left(\frac{u_0}{3000\,\mathrm{km\ s^{-1}}}\right)^2\left(\frac{R_{tot}}{4}\right)^{-2}\mathrm{keV}\ . \quad (9)$$

At frequencies lower than ν_2:

$$\Delta R_2(\nu < \nu_2) \simeq L^{\rm loss}_{\rm adv} = \frac{u_0}{R_{tot}}\tau_l(p) \propto \nu^{-1/2}\ , \quad (10)$$

while for $\nu > \nu_2$ the downstream emission comes from a region of constant size:

$$\Delta R_2(\nu > \nu_2) \simeq L^{\rm loss}_{\rm diff} = 4.5\times10^{17}\left(\frac{B_2}{40\mu\mathrm{G}}\right)^{-\frac{3}{2}}\mathrm{cm}\ . \quad (11)$$

In order to compare ΔR_1 and ΔR_2 with the observed rim thickness, we need to take into account projection effects. Let us define the observed thickness, $\Delta R^{\rm obs}_{1(2)}$, as the width over which the emissivity drops to half the peak value. Assuming spherical geometry, an emission profile $I_\nu \propto \exp[-x/\Delta R]$ and $\Delta R_{1(2)}$ much smaller than the SNR radius, the observed widths are $\Delta R^{\rm obs}_1 = 0.7\Delta R_1$ and $\Delta R^{\rm obs}_2 = 4.6\Delta R_2$. Hence projection effects make the observed width of the downstream emission region appear larger than the physical one.

When we observe the filaments at frequencies $\nu > \nu_1, \nu_2$, the ratio between the observed thickness downstream and upsteam can be estimated as:

$$\frac{\Delta R^{\rm obs}_2}{\Delta R^{\rm obs}_1} = \frac{4.6\,L^{\rm loss}_{\rm diff}}{0.7\,L_{\rm diff}(p_{e,\rm max})} = 12\sqrt{\frac{1+R_B R_{tot}U_p}{R_B^3(1-R_{tot}^{-1}U_p^{-1})}}\ , \quad (12)$$

where the last equality is obtained using the full expression for $H(p)$ that appears in Eq. 2 (see Eq. (4) of Morlino et al. 2009). Remarkably this result is independent of magnetic field strength, shock speed and electron energy, while it only depends on the compression ratios (magnetic compression at the subshock R_B and total compression R_{tot}) and on $U_p = u_p/u_0$. Since $R_{sub}/R_{tot} \leqslant U_p \leqslant 1$ and $\sqrt{11} \leqslant R_B \leqslant 4$, using reasonable values for R_{tot} the ratio $\Delta R^{\rm obs}_2/\Delta R^{\rm obs}_1$ is always between 6 and 8. Since the rim in SN 1006 has an overall width of 30"-40" for $\nu \gtrsim \nu_1, \nu_2$, the result above implies that the upstream halo should have an observed width of $\lesssim 6''$.

4 COMPARISON BETWEEN THEORY AND OBSERVATIONS

Our model of NLDSA contains four free parameters, namely: the density of the unshocked ISM, n_0, the shock speed, u_0, the proton injection efficiency, ξ, and the relative normalization between electron and proton spectra, K_{ep}. SN 1006 is thought to be the remnant of a type Ia SN explosion and to expand in a fairly uniform ISM. We

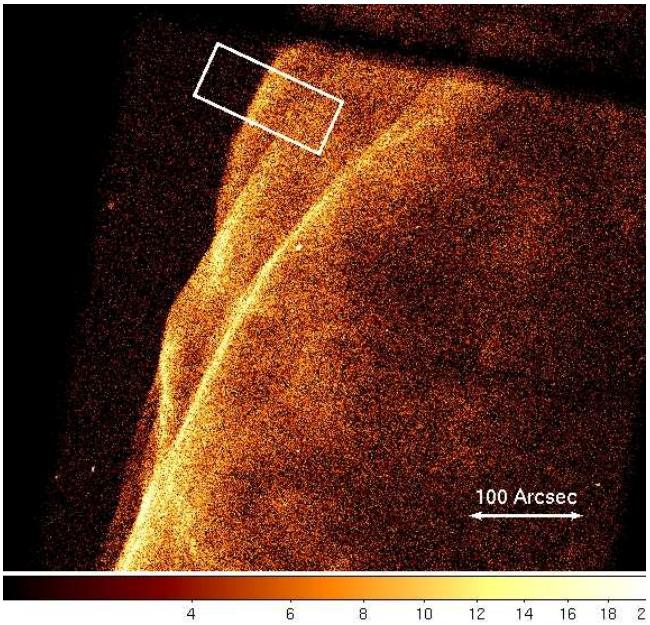

Figure 1. *Chandra* X-ray image of the northeastern limb showed in squared root color scale. The white rectangle ($50'' \times 120''$) is the region used to extract the X-ray radial profile plotted in Fig. 2.

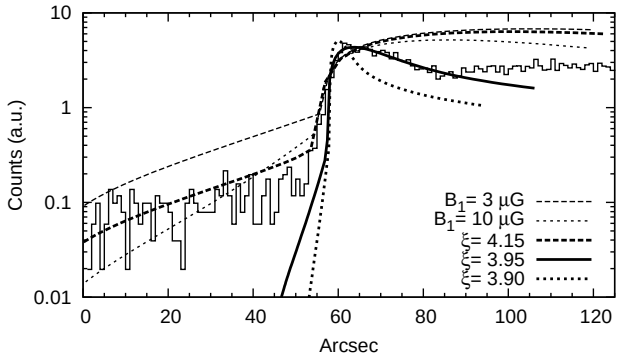

Figure 2. Radial profile of the emission in the 0.8-2.0 keV band, extracted from the rectangular region in Fig. 1 (*thin black line*). Overplotted are the theoretical predictions of NLDSA for 3 different injection efficiencies (*thick lines*) and those of test-particle theory for two different values of the pre-existing turbulent magnetic field upstream (*thin lines*).

adopt $n_0 = 0.05\,\mathrm{cm}^{-3}$, based on the measurement by Acero et al. (2007) (also consistent with a hadronic interpretation of the TeV emission recently detected by H.E.S.S.; see Berezhko, Ksenofontov & Völk 2009). We estimate the shock speed using a code for the evolution of type Ia SNRs (Caprioli, Amato & Blasi 2010), fixing the explosion energy and the mass of the ejecta to the standard values $E_{\rm SN} = 10^{51}$erg and $M_{eje} = 1.4 M_\odot$. Once n_0 is fixed, given the known age of the remnant, we estimate $u_0 = 4330$km/s and a radius $R_{\rm SNR} = 7.7$ pc. Comparing this latter value with the observed angular diameter of 30', the inferred distance of SN 1006 is $d = 1.77$ kpc. This makes our estimate of u_0 in remarkable agreement with recent measurements

Table 1.

ξ	B_1 (μG)	B_2 (μG)	R_{sub}	R_{tot}
3.90	47	175	3.78	6.39
3.95	23	90	3.93	5.53
4.15	5.3	21	4.00	4.08
∞	3.0	10	4.00	4.00
∞	10	33	4.00	4.00

of the proper motion of X-ray filaments by Katsuda et al. (2009), which give $u_0 = 4670\,(d/2\,\mathrm{kpc})$ km/s.

We extract the X-ray emission profile from recent *Chandra* observations (2008 June 24; ObsID.9107; PI: Petre; see Katsuda et al. 2009). Fig. 1 shows the *Chandra* image of the northeastern limb. We selected the rectangular region of $50'' \times 120''$ highlighted by the white box in the figure, so as to exclude regions where multiple shocks overlap. The resulting radial profile, in the energy band 0.8-2.0 keV, is plotted as a histogram in Fig. 2 and is in good agreement with that of Long et al. (2003).

The curves in Fig. 2 refer to different values of the injection parameter $\xi = 3.90$, 3.95, 4.15 and $B_0 = 3\mu G$. The two curves labelled as $B_1 = 3\mu G$ and $10\mu G$ are test particle cases with a turbulent magnetic field as indicated, and with the perpendicular components compressed at the shock, so that $B_2 = \sqrt{11} B_1$. In the other cases the magnetic field at a position x in the precursor is calculated as described by Eq. (5), and then compressed at the subshock, resulting in the values of B_1 and B_2 reported in Table 1, together with the compression factors R_{sub} and R_{tot}.

It is clear that DSA in the test particle regime cannot explain either the radial profile in the precursor or that in the downstream region, although the latter might still be explained by requiring some magnetic damping. The intermediate case, $\xi = 4.15$, which corresponds to modest injection, is also inappropriate for the same reasons. Moreover, the test particle and the inefficient cases show a potentially detectable precursor, which is however not observed. Remarkably, the solution with $\xi = 3.95$ (corresponding to $B_2 \simeq 90\mu G$) fits well the downstream X-ray profile and shows a modest upstream halo that is however fully consistent with the observations. For larger injection efficiencies the upstream halo becomes smaller than the *Chandra* resolution, but the predicted downstream rim is too narrow compared with observations.

5 DISCUSSION AND CONCLUSIONS

We studied the observed radial profile of the X-ray emission in SN 1006 in the context of the theory of NLDSA. We concentrated our attention on a filament of X-ray emission which was already studied by Long et al. (2003) since it shows a pronounced jump in emission by a factor ~ 70 at what appears to be the shock surface. This filament is rather clean from the observational point of view, in that there seems to be only one shock surface within the observed slice.

The conclusions of our investigation can be summarized as follows:

1) The radial profile of the X-ray emission is very well described within the context of NLDSA, as a consequence of a large magnetic field amplification upstream of the shock. This scenario describes both the downstream narrow filament and the non detection of a precursor upstream of the shock. The main reason for this non-detection is that the magnetic field upstream becomes strong enough to make the diffusion/loss region of electrons comparable with the angular resolution of *Chandra*. Moreover, if magnetic field is amplified upstream through the excitation of a streaming instability, the gradient in the precursor magnetic field makes the size of the X-ray emission even smaller.

Fixing $n_0 = 0.05\,\mathrm{cm}^{-3}$, we best fit the observed radial profile with $\xi = 3.95$ which implies a CR acceleration efficiency of ~ 29 per cent and an electron/proton ratio $K_{ep} \sim 1.3\,10^{-4}$. An inefficient scenario of CR acceleration appears to be inadequate to fit observations: the narrow filaments would require some level of magnetic field damping downstream, which however does not seem to be compatible with the absence of filaments in the radio band (Rothenflug et al. 2004). Upstream, the inefficient scenario typically leads to broader emission regions than observed by *Chandra*.

We stress that our conclusions do not strongly depend on the assumed values of the upstream magnetic field and shock speed. An equally good fit of the X-ray radial profile can be obtained for $B_0 = 5\mu G$ (about the highest reasonable value at the galactic latitude of SN1006) and for a shock velocity of 4670 km/s corresponding to a larger distance of the remnant ($d = 2$kpc) and to an exposion energy of $1.5 \cdot 10^{51}$erg. For a magnetic field strength $B_0 = 5\mu G$ the best-fit injection parameter needs to be changed ($\xi = 3.98$), corresponding to a slightly smaller acceleration efficiency. For a shock velocity of 4670 km/s a fit can be obtained for $\xi = 3.93$.

2) Our conclusions are in disagreement with the point made by Long et al. (2003) that one needs a jump in the magnetic field at the shock which is $\gg 4$, equivalent to MFA downstream. We find that the important ingredient is that there is MFA upstream, as also found by Berezhko et al. (2003), although adopting values of the ambient density and shock velocity that have now been excluded by observations (Acero et al. 2007). Our calculations show that in the case of SN 1006, inclusion of MFA *a la* Bell & Lucek (2001) (which would further enhance the magnetic field *upstream*) is not necessary.

3) Contrary to Berezhko et al. (2003) we think that an efficient CR acceleration is not *the only reasonably thinkable condition* to explain the X-ray observations. The non detection of a CR precursor upstream can also be attributed, at least qualitatively, to the presence of a quasi-perpendicular magnetic field, as was also inferred by Bamba et al. (2003) (even if their conclusions were based on the incorrect assumption of no magnetic jump at the shock surface); in this case CRs can be accelerated to rather high energies (Jokipii 1987). In this situation the magnetic field could be amplified downstream of the shock as due to fluid instabilities if the shock propagates in a inhomogeneous medium (e.g. Giacalone & Jokipii 2007). Whether this configuration can explain the details of the X-ray radial profile should be subject of a dedicated investigation.

ACKNOWLEDGMENTS

This work was partially supported by MIUR (grant PRIN2006) and by ASI through contract ASI-INAF I/088/06/0. This research was also supported in part by the National Science Foundation under Grant No. PHY05-51164. We wish to acknowledge the KITP in Santa Barbara for the exciting atmosphere during the Program Particle Acceleration in Astrophysical Plasmas, July 26-October 3, 2009. GM whish to thank Daniel Patnaude for helpful suggestions in handling the *Chandra* data.

REFERENCES

Acero, F., Ballet, J. & Decourchelle, A., 2007, A&A, 475, 883
Amato, E., Blasi, P., 2005, MNRAS, 364, L76
Amato, E., Blasi, P., 2006, MNRAS, 371, 1251
Amato, E., Blasi, P., 2009, MNRAS, 392, 1591
Ballet, J., 2006, Adv. Sp. Res., 37, 1902
Bamba, A., Yamazaki, R., Ueno, M., Koyama, K., 2003, ApJ, 589, 827B
Bell, A. R., 2004, MNRAS, 353, 550
Bell, A. R., Lucek, S. G., 2001, MNRAS, 321, 433
Berezhko, E. G., Ksenofontov, L. T. & Völk, H. J. 2009, A&A, 505, 169
Berezhko, E. G., Ksenofontov, L. T., Völk, H. J., 2003, A&A, 412, L11
Blasi, P., 2009, MNRAS, *submitted* (Preprint arXiv0912.2053)
Blasi, P., Amato, E., Caprioli, D., 2007, MNRAS, 375, 1471
Blasi, P., Gabici, S. & Vannoni, G., 2005, MNRAS, 361, 907
Caprioli, D., Blasi, P., Amato, E. & Vietri, M., 2009, MNRAS, 395, 895
Caprioli, D., Amato, E., Blasi, P., 2010, APh, 33, 160 (Preprint arXiv0912.2964)
Jokipii, J. R., 1987, ApJ, 313, 842
Giacalone, J., & Jokipii, J. R., 2007, ApJ, 663, L41
Katsuda, S., Petre, R., Long, K. S., Reynolds, S. P., Winkler, P. F., Mori, K., Tsunemi, H., 2009, ApJ, 692, L105
Long, K. S., Reynolds, S. P., Raymond, J. C., Winkler, P. F., Dyer, K. K. & Petre, R., 2003, ApJ, 586, 1162
Morlino, G., Amato, E. and Blasi, P., 2009, MNRAS, 392, 240
Parizot, E., Marcowith, A., Ballet, J. and Gallant, Y. A., 2006, A&A, 453, 387
Pohl, M., Yan, H., & Lazarian, A., 2005, ApJ, 626, L101
Rothenflug, R., Ballet, J., Dubner, G., Giacani, E., Decourchelle, A., Ferrando, P., 2004, A&A, 425, 121
Skilling, J., 1975, MNRAS, 172, 557
Zirakashvili, V. N. & Aharonian, F., 2007, A&A, 465, 695